Constraints on cosmic strings using data from the first Advanced LIGO observing run

B. P. Abbott *et al.*[*]
(LIGO Scientific Collaboration and Virgo Collaboration)

(Received 4 December 2017; published 8 May 2018)

Cosmic strings are topological defects which can be formed in grand unified theory scale phase transitions in the early universe. They are also predicted to form in the context of string theory. The main mechanism for a network of Nambu-Goto cosmic strings to lose energy is through the production of loops and the subsequent emission of gravitational waves, thus offering an experimental signature for the existence of cosmic strings. Here we report on the analysis conducted to specifically search for gravitational-wave bursts from cosmic string loops in the data of Advanced LIGO 2015-2016 observing run (O1). No evidence of such signals was found in the data, and as a result we set upper limits on the cosmic string parameters for three recent loop distribution models. In this paper, we initially derive constraints on the string tension $G\mu$ and the intercommutation probability, using not only the burst analysis performed on the O1 data set but also results from the previously published LIGO stochastic O1 analysis, pulsar timing arrays, cosmic microwave background and big-bang nucleosynthesis experiments. We show that these data sets are complementary in that they probe gravitational waves produced by cosmic string loops during very different epochs. Finally, we show that the data sets exclude large parts of the parameter space of the three loop distribution models we consider.

DOI: 10.1103/PhysRevD.97.102002

I. INTRODUCTION

The recent observation of gravitational waves [1] (GWs) has started a new era in astronomy [2,3]. In the coming years Advanced LIGO [4] and Advanced Virgo [5] will be targeting a wide variety of GW sources [6]. Some of these potential sources could yield new physics and information about the Universe at its earliest moments. This would be the case for the observation of GWs from cosmic strings, which are one-dimensional topological defects, formed after a spontaneous symmetry phase transition characterized by a vacuum manifold with noncontractible loops. Cosmic strings were first introduced by Kibble [7] (for a review see for instance [8–10]). They can be generically produced in the context of grand unified theories [11]. Linear-type topological defects of different forms should leave a variety of observational signatures, opening up a fascinating window to fundamental physics at very high energy scales. In particular, they should lens distant galaxies [12–14], produce high energy cosmic rays [15], lead to anisotropies in the cosmic microwave background [16,17], and produce GWs [18,19].

A network of cosmic strings is primarily characterized by the string tension $G\mu$ ($c = 1$), where G is Newton's constant and μ the mass per unit length. The existence of cosmic strings can be tested using the cosmic microwave background (CMB) measurements. Confronting experimental CMB data with numerical simulations of cosmic string networks [20–23], the string tension is constrained to be smaller than a few 10^{-7}.

Cosmic superstrings are coherent macroscopic states of fundamental superstrings (F-strings) and also D-branes extended in one macroscopic direction (D-strings). They are predicted in superstring inspired inflationary models with spacetime-wrapping D-branes [24,25]. For cosmic superstrings, one must introduce another parameter to account for the fact that they interact probabilistically. In [26], it is suggested that this intercommutation probability p must take values between 10^{-1} and 1 for D-strings and between 10^{-3} and 1 for F-strings. In this paper, we will refer to both topological strings and superstrings as "strings," and parametrize them by p and $G\mu$.

Cosmic string parameters can also be accessed through GWs. Indeed, the dynamics of the network is driven by the formation of loops and the emission of GWs. In particular, cusps and kinks propagating on string loops are expected to produce powerful bursts of GWs. The superposition of these bursts gives rise to a stochastic background which can be probed over a large range of frequencies by different observations. Historically, the big-bang nucleosynthesis (BBN) data provided the first constraints on cosmic strings [27]. It was then surpassed by CMB bounds [28] to then be surpassed more recently by pulsar timing bounds [29]. In this paper, we report on the search for GW burst signals

[*]Full author list given at the end of the article.

produced by cosmic string cusps and kinks using Advanced LIGO data collected between September 12, 2015 06:00 UTC and January 19, 2016 17:00 UTC [30], offering a total of $T_{\rm obs} = 4\,163\,421$ s (∼48.2 days) of coincident data between the two LIGO detectors. Moreover, combining the result from the stochastic GW background search previously published in [31], we test and constrain cosmic string models. While the LIGO O1 burst limit remains weak, the stochastic bound now surpasses the BBN bound for the first time and is competitive with the CMB bound across much of the parameter space.

We will place constraints on the most up-to-date string loop distributions. In particular, we select three analytic cosmic string models ($M = \{1, 2, 3\}$) [8,32–35] for the number density of string loops, developed in part from numerical simulations of Nambu-Goto string networks (zero thickness strings with intercommutation probability equal to unity), in a Friedman-Lemaître-Robertson-Walker geometry. These models are more fully described in Sec. II where their fundamental differences are also discussed. Section III presents an overview of the experimental data sets which are used to constrain the cosmic string parameters. Finally, the resulting limits are discussed in Sec. IV.

II. COSMIC STRING MODELS

We constrain three different models of cosmic strings indexed by M. Common to all these models is the assumption that the width of the strings is negligible compared to the size of the horizon, so that the string dynamics is given by the Nambu-Goto action. A further input is the strings intercommutation probability p. For field theory strings, and in particular $U(1)$ Abelian-Higgs strings in the Bogomol'nyi–Prasad–Sommerfield limit [8], intercommutation occurs with effective unit probability [36,37], $p = 1$. That is, when two superhorizon (infinite) strings intersect, they always swap partners; and if a string intersects itself, it therefore chops off a (subhorizon) loop. The latter can also result from string-string intersections at two points, leading to the formation of two new infinite strings and a loop.

Cosmic string loops oscillate periodically in time, emitting GWs.[1] A loop of invariant length ℓ has period $T = \ell/2$ and corresponding fundamental frequency $\omega = 4\pi/\ell$. As a result it radiates GWs with frequencies which are multiples of ω, and decays in a lifetime $\tau = \ell/\gamma_{\rm d}$ where [18,40,41]

$$\gamma_{\rm d} \equiv \Gamma G\mu \quad \text{with} \quad \Gamma \simeq 50. \tag{1}$$

If a loop contains kinks [41–43] (discontinuities on the tangent vector of a string) and cusps (points where the string instantaneously reaches the speed of light), these source bursts of beamed GWs [44–46]. The incoherent superposition of these bursts give rise to a stationary and nearly Gaussian stochastic GW background. Occasionally, sharp and high-amplitude bursts of GWs stand above this stochastic GW background.

The three models considered here differ in the loop distribution $n(\ell, t)d\ell$, namely the number density of cosmic string loops of invariant length between ℓ and $\ell + d\ell$ at cosmic time t. To determine the consequences of these differences on their GW signal, we work in units of cosmic time t and introduce the dimensionless variables

$$\gamma \equiv \ell/t \quad \text{and} \quad \mathcal{F}(\gamma, t) \equiv n(\ell, t) \times t^4. \tag{2}$$

We will often refer to γ as the relative size of loops and $\mathcal{F}$ as simply the loop distribution. All GWs observed today are formed when the string network is in its *scaling regime*, namely a self-similar, attractor solution in which all the typical length scales in the problem are proportional to cosmic time.[2]

The models considered here were developed (in part) using numerical simulations of Nambu-Goto strings, for which $p = 1$. As mentioned above, cosmic superstrings intercommute with probability $p < 1$. The effect of a reduced intercommutation probability on the loop distribution has been studied in [47]. Following this reference we take[3] $\mathcal{F}_{p<1} = \mathcal{F}/p$, leading to an increased density of strings [48] and to an enhancement of various observational signatures.

A. Model $M = 1$: Original large loop distribution

The first model we consider is the oldest, developed in [8,32]. It assumes that, in the scaling regime, all loops chopped off the infinite string network are formed with the *same* relative size, which we denote by α. At time t, the distribution of loops of length ℓ to $\ell + d\ell$ contains loops chopped off the infinite string network at earlier times, and diluted by the expansion of the Universe and by the emission of GWs. Assuming that loops do not self-intersect once formed, and taking into account that the length of a loop decays at the rate $d\ell/dt = -\gamma_{\rm d}$, the scaling loop distribution (for $\gamma \leq \alpha$) in the radiation era is given by [8]

$$\mathcal{F}^{(1)}_{\rm rad}(\gamma) = \frac{C_{\rm rad}}{(\gamma + \gamma_{\rm d})^{5/2}}\Theta(\alpha - \gamma), \tag{3}$$

where Θ is the Heaviside function, and the superscript (1) stands for model $M = 1$. Some of these loops formed in the radiation era can survive into the matter era, meaning

[1] Superhorizon cosmic strings also emit GWs, due to their small-scale structure [19,38,39].

[2] Scaling breaks down for a short time in the transition between the radiation and matter eras, and similarly in the transition to dark energy domination.

[3] In [47] the exponent of the power-law behavior was found to be slightly different, namely 0.6. Since our goal here is to highlight the effect of $p < 1$, we used a simple dependence of $1/p$ as many others in the literature have done.

that in the matter era the loop distribution has two components. Those loops surviving from the radiation era have distribution

$$\mathcal{F}^{(1),a}_{\rm mat}(\gamma,t)=\frac{C_{\rm rad}}{(\gamma+\gamma_{\rm d})^{5/2}}\left(\frac{t_{\rm eq}}{t}\right)^{1/2}\Theta(-\gamma+\beta(t)), \quad (4)$$

with $t_{\rm eq}$ the time of the radiation to matter transition, and where the lower bound, $\beta(t)$, is the length in scaling units, of the last loops formed in the radiation era at time $t_{\rm eq}$:

$$\beta(t)=\alpha\frac{t_{\rm eq}}{t}-\gamma_{\rm d}\left(1-\frac{t_{\rm eq}}{t}\right). \quad (5)$$

The loops formed in the matter era itself have a distribution

$$\mathcal{F}^{(1),b}_{\rm mat}(\gamma,t)=\frac{C_{\rm mat}}{(\gamma+\gamma_{\rm d})^{2}}\Theta(\alpha-\gamma)\Theta(\gamma-\beta(t)). \quad (6)$$

The normalization constants $C_{\rm rad}$ and $C_{\rm mat}$ cannot be determined from analytical arguments, but rather are fixed by matching with numerical simulations of Nambu-Goto strings. Following [8,32], we set them to

$$C_{\rm rad}\simeq 1.6, \qquad C_{\rm mat}\simeq 0.48. \quad (7)$$

Furthermore we shall assume that $\alpha\simeq 0.1$. The loop distribution in the matter era is thus given by the sum of distributions in Eqs. (4) and (6).

The loop distribution $\mathcal{F}^{(1)}$ is plotted in Fig. 1 for different redshift values and fixing $G\mu$ at 10^{-8}. A discontinuity, visible for low redshift values, results from the radiation-matter transition which is modeled by Heaviside functions. For $t<t_{eq}$, the loop distribution is entirely determined by Eq. (3) and is time independent.

B. Model $M=2$: Large loop Nambu-Goto distribution of Blanco-Pillado *et al.*

Rather than postulating that all loops are formed with a given size αt at time t as in model 1, the loop production function can be determined from numerical simulations. This approach was taken in [33], determining the rate of production of loops of size ℓ and momentum $\vec{p}$ at time t. Armed with this information, $n(\ell,t)$ is determined analytically as in model 1 with the additional assumption that the momentum dependence of the loop production function is weak so that it can be integrated out.

In the radiation era, the scaling distribution reads

$$\mathcal{F}^{(2)}_{\rm rad}(\gamma)=\frac{0.18}{(\gamma+\gamma_{\rm d})^{5/2}}\Theta(0.1-\gamma), \quad (8)$$

where the superscript (2) stands for model 2. In the matter era, analogously to above, there are two contributions. The loops left over from the radiation era can be deduced from above, whereas loops formed in the matter era have distribution

$$\mathcal{F}^{(2),b}_{\rm mat}(\gamma,t)=\frac{0.27-0.45\gamma^{0.31}}{(\gamma+\gamma_{\rm d})^{2}}\Theta(0.18-\gamma)\Theta(\gamma-\beta(t)), \quad (9)$$

where $\beta(t)$ is given in Eq. (5) with $\alpha=0.1$.

The loop distribution of model 2 is plotted in Fig. 1. Notice that in the radiation era, the distributions in models 1 and 2 take the same functional form, though their normalization differs by a factor of order 10. In the matter era, the functional form is slightly different and the normalization is smaller by a factor of order 2. The authors of [33] attribute this reduction in the number of loops to two effects: (i) only about 10% of the power is radiated into large loops—indeed, most of it is lost directly into smaller loops which radiate away very quickly; (ii) most of the energy leaving the network goes into loop kinetic energy which is lost to redshifting.

C. Model $M=3$: Large loop Nambu-Goto distribution of Ringeval *et al.*

This analytical model was presented in [34], and is based in part on the numerical simulations of [35].

As opposed to model 2, here the (different) numerical simulation is not used to determine the loop production function at time t, but rather the distribution of non-self-intersecting loops at time t. The analytical modeling also differs from that of model 2 in that an extra ingredient is

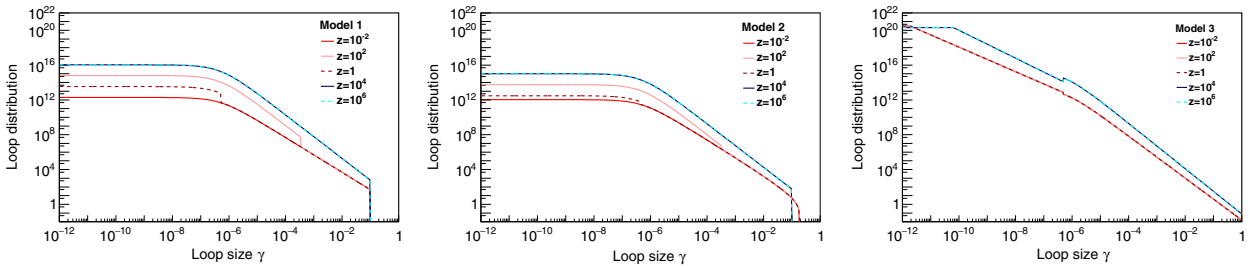

FIG. 1. Loop size distributions predicted by three models: $M=1,2,3$. For each model, the loop distribution, $\mathcal{F}(\gamma,t(z))$, is plotted for different redshift values and fixing $G\mu$ at 10^{-8}.

added: not only do loops emit GWs—which decreases their length ℓ—but this GW emission backreacts on the loops. Backreaction smooths out the loops on the smallest scales (in particular any kinks), thus hindering the formation of smaller loops [43,49]. Hence, the distributions of models 2 and 3 differ for the smallest loops.

Physically, therefore, the model of [34] contains a further length scale γ_c, the so-called "gravitational backreaction scale," with

$$\gamma_c < \gamma_d,$$

where γ_d is the gravitational decay scale introduced above. Following the numerical simulation of [35],

$$\gamma_c = \Upsilon(G\mu)^{1+2\chi} \quad \text{where } \Upsilon \sim 10 \quad \text{and} \quad \chi = 1 - P/2, \tag{10}$$

with

$$P = 1.41^{+0.08}_{-0.07}|_{\rm mat}, \qquad P = 1.60^{+0.21}_{-0.15}|_{\rm rad}. \tag{11}$$

The resulting distribution of loops is given in [34]. In this paper, we work with the asymptotic expressions given in Sec. II. 4 of [34], valid in the scaling regime ($t \gg t_{\rm ini}$). Hence the contribution of those loops formed in the radiation era, but which persist into the matter era, are neglected. The loop distribution has three distinct regimes with different power-law behaviors, depending on whether the loops are smaller than γ_c ($\gamma \le \gamma_c$), of intermediate length ($\gamma_c \le \gamma \le \gamma_d$), or larger than γ_d (that is $\gamma_d \le \gamma \le \gamma_{\rm max}$). Here $\gamma_{\rm max} = 1/(1-\nu)$ is the largest allowed (horizon-sized) loop, in units of cosmic time, where the power-law time evolution of the scale factor of the universe, $a \sim t^\nu$, is

$$\nu = \frac{2}{3}\bigg|_{\rm mat}, \qquad \nu = \frac{1}{2}\bigg|_{\rm rad}. \tag{12}$$

Hence, $\gamma_{\rm max} = 2$, or $\gamma_{\rm max} = 3$, depending on whether we are in the radiation-dominated or matter-dominated era, respectively. More explicitly,

(i) for loops with length scale large compared to γ_d

$$\mathcal{F}^{(3)}(\gamma_d \ll \gamma < \gamma_{\rm max}) \simeq \frac{C}{(\gamma+\gamma_d)^{P+1}}; \tag{13}$$

(ii) for loops with length scale in the range $\gamma_c < \gamma \ll \gamma_d$:

$$\mathcal{F}^{(3)}(\gamma_c < \gamma \ll \gamma_d) \simeq \frac{C(3\nu - 2\chi - 1)}{2-2\chi}\frac{1}{\gamma_d}\frac{1}{\gamma^P}; \tag{14}$$

(iii) for loops with length scale smaller than γ_c the distribution is γ independent:

$$\mathcal{F}^{(3)}(\gamma \ll \gamma_c \ll \gamma_d) \simeq \frac{C(3\nu - 2\chi - 1)}{2-2\chi}\frac{1}{\gamma_c^P}\frac{1}{\gamma_d}. \tag{15}$$

Here, C is given by

$$C = C_0(1-\nu)^{3-P} \tag{16}$$

where

$$C_0 = 0.09^{-0.03}_{+0.03}|_{\rm mat}, \qquad C_0 = 0.21^{-0.12}_{+0.13}|_{\rm rad}. \tag{17}$$

In the case of large loops [Eq. (13)], C normalizes the distribution. In the radiation era where $\nu = 1/2$,

$$C \sim 0.08 \qquad \text{(radiation)}$$

(a factor of about 20 smaller than model 1), and in the matter era where $\nu = 2/3$,

$$C \sim 0.016 \qquad \text{(matter)}$$

(a factor of about 30 smaller than model 1).

The three loop regimes are well visible when plotting the loop distribution: see Fig. 1. Regarding the GW signal, the most significant difference between model 3 and the two previous models is in the very small loop regime ($\gamma \ll \gamma_c$). Comparing Eq. (15) with Eqs. (4) and (8), for models 3, 1, and 2 respectively, in the radiation era, we find

$$\frac{\mathcal{F}^{(3)}}{\mathcal{F}^{(1,2)}}\bigg|_{\gamma \ll \gamma_c} \propto (G\mu)^{-0.74}, \tag{18}$$

where the proportionality constant is 2.5×10^{-2} for model 1 and approximately ten times larger for model 2. For a typical value of $G\mu = 10^{-8}$, and relative to model 1, there are $\sim 2 \times 10^4$ more very small loops in the radiation era in model 3. As we will see in Sec. III, such a high number of small loops in model 3 will have important consequences in the rate of GW events we can detect and on the amplitude of the stochastic gravitational wave background.

III. CONSTRAINING COSMIC STRINGS MODELS WITH GW DATA

A. Gravitational waves from cosmic strings

GW bursts are emitted by both cusps and kinks on cosmic string loops, the frequency-domain waveform of which was calculated in [44,45,50]:

$$h(\ell, z, f) = A_q(\ell, z) f^{-q} \Theta(f_h - f)\Theta(f - f_\ell), \tag{19}$$

where $q = 4/3$ for cusps, $q = 5/3$ for kinks, and $A_q(\ell, z)$ is the signal amplitude produced by a cusp/kink

propagating on a loop of size ℓ at redshift z. This waveform is linearly polarized and is only valid if the beaming angle

$$\theta_m(\ell, z, f) \equiv (g_2 f(1+z)\ell)^{-1/3} < 1. \tag{20}$$

Here g_2 is an ignorance factor assumed to be 1 in this work (see [32]). In order to detect the GW, the angle subtended by the line of sight and the cusp/kink on a loop of typical invariant length ℓ at redshift z must be smaller than θ_m. This condition then determines the high-frequency cutoff f_h in Eq. (19). The low-frequency cutoff f_ℓ—though in principle determined by the kink amplitude, or by the size of the feature that produces the cusp—is in practice given by the lower end of the GW detector's sensitive band. The amplitude $A_q(\ell, z)$ is given by [44]

$$A_q(\ell, z) = g_1 \frac{G\mu\ell^{2-q}}{(1+z)^{q-1} r(z)}, \tag{21}$$

where the proper distance to the source is given by $r(z) = H_0^{-1}\varphi_r(z)$. Here, H_0 is the Hubble parameter today and $\varphi_r(z)$ is determined in terms of the cosmological parameters and expressed in Appendix A. Finally g_1 gathers together a certain number of uncertainties which enter into the calculation of the cusp and kink waveform (including the amplitude of the cusp/kink, as well as numerical factors of order 1; see [32,44]). We will set $g_1 = 1$. In the following, we will use Eq. (21) to conveniently choose two variables out of ℓ, z, and A_q. Similarly, we will use Eq. (19) to substitute A_q for the strain amplitude h.

For a given loop distribution model M, in the following we use the GW burst rate derived in [32] and recalled in Appendix B

$$\frac{d^2R_q^{(M)}}{dzdh}(h, z, f) = \frac{2N_q H_0^{-3}\varphi_V(z)}{(2-q)(1+z)ht^4(z)} \times \mathcal{F}^{(M)}\left(\frac{\ell(hf^q, z)}{t(z)}, t(z)\right) \times \Delta_q(hf^q, z, f). \tag{22}$$

The first two lines on the right-hand side give the number of cusp/kink features per unit space-time volume on loops of size ℓ, where N_q is the number of cusps/kinks per oscillation period $T = \ell/2$ of the loop. In this paper, the number of cusps/kinks per loop oscillation is set to 1 although some models [51] suggest that this number can be much larger than one. Cosmic time is given by $t(z) = \varphi_t(z)/H_0$ and the proper volume element is $dV(z) = H_0^{-3}\varphi_V(z)dz$ where $\varphi_t(z)$ and $\varphi_V(z)$ are given in Appendix A. Finally Δ_q, which is fully derived in Appendix B, is the fraction of GW events of amplitude A_q that are observable at frequency f and redshift z.

B. Gravitational-wave bursts

We searched the Advanced LIGO O1 data (2015–2016) [30] for individual bursts of GWs from cusps and kinks. The search for cusp signals was previously conducted using initial LIGO and Virgo data and no signal was found [52].

For this paper, we use the same analysis pipeline to search for both cusp and kink signals. We perform a Wiener-filter analysis to identify events matching the waveform predicted by the theory [44,45,50] and given in Eq. (19). GW events are detected by matching the data to a bank of waveforms parametrized by the high-frequency cutoff f_h, with 30 Hz $< f_h <$ 4096 Hz. Then resulting events detected at LIGO-Hanford and at LIGO-Livingston are set in time coincidence to reject detector noise artifacts mimicking cosmic string signals. Finally, a multivariate likelihood ratio [53] is computed to rank coincident events and infer probability to be signal or noise. The analysis method is described in [52]. In this paper we only report on the results obtained from the analysis of new O1 LIGO data.

The upper plots in Fig. 2 present the final event rate as a function of the likelihood ratio Λ for the cusp and kink search. The rate of accidental coincident events between the two detectors (background) is estimated by performing the analysis over 6000 time-shifted LIGO-Livingston data sets. This background data set virtually offers 2.5×10^{10} s (~790.7 years) of double-coincidence time. For both cusps and kinks, the candidate ranking values are compatible with the expected background distribution, so no signal was found. The highest-ranked event is measured with $\Lambda_h \simeq 232$ for cusps and $\Lambda_h \simeq 611$ for kinks. These events were scrutinized and were found to belong to a known category of noise transients called "blips" described in [54], matching very well the waveform of cusp and kink signals.

The sensitivity to cusp and kink GW events is estimated experimentally by injecting simulated signals of known amplitude A_q in the data. We measure the detection efficiency $e_q(A_q)$ as the fraction of simulated signals recovered with $\Lambda > \Lambda_h$, which is associated to a false alarm rate of $1/T_{\rm obs} = 2.40 \times 10^{-7}$ Hz. The detection efficiencies are displayed in the bottom plots in Fig. 2. The sensitivity curve of the 2005–2010 LIGO-Virgo cusp search is also plotted, and should be compared with the O1 LIGO sensitivity measured for an equivalent false-alarm rate of 1.85×10^{-8} Hz [52]. The sensitivity to cosmic string signals is improved by a factor 10. This gain is explained by the significant sensitivity improvement at low frequencies of Advanced detectors [30].

Since no signal from cosmic string was found in LIGO O1 data, it is possible to constrain cosmic string parameters using models 1, 2 and 3. To generate statistical statements about our ability to detect true GW signals, we adopt the loudest event statistic [55]. We compute an effective detection rate for a given loop distribution model M:

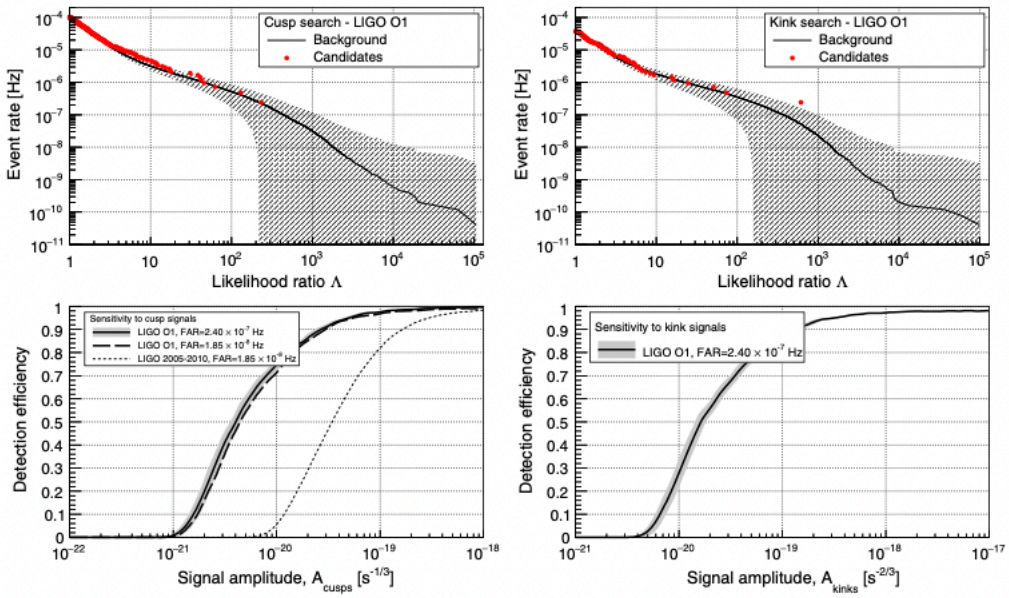

FIG. 2. In the upper plots, the red points show the measured cumulative cusp (left-hand plot) and kink (right-hand plot) GW burst rate (using $T_{\rm obs}$ as normalization) as a function of the likelihood ratio Λ. The black line shows the expected background of the search with the $\pm 1\sigma$ statistical error represented by the hatched area. In both cases, the highest-ranked event ($\Lambda_h \simeq 232$ and $\Lambda_h \simeq 611$) is consistent with the background. The lower plots show the sensitivity of the search as a function of the cusp/kink signal amplitude. This is measured by the fraction of simulated cusp/kink events recovered with $\Lambda > \Lambda_h$. The sensitivity to cusp signals is also measured for a false-alarm rate (FAR) of 1.85×10^{-6} Hz to be compared with the sensitivity of the previous LIGO-Virgo burst search [52] (dashed lines).

$$\mathcal{R}_q^{(M)}(G\mu, p) = \int_0^{+\infty} dA_q e_q(A_q) \tag{23}$$

$$\times \int_0^{+\infty} dz \frac{d^2 R_q^{(M)}}{dz dA_q}(A_q, z, f^*; G\mu, p), \tag{24}$$

where the predicted rate is given by Eq. (22) with the change of variables $A_q = hf^{-q}$. The frequency $f^* = 30$ Hz is the lowest high-frequency cutoff used in the search template bank as it provides the maximum angle between the line of sight and the cusp/kink on the loop. The parameter space of model M, $(G\mu, p)$, is scanned and excluded at a 95% level when $\mathcal{R}_q^{(M)}$ exceeds $2.996/T_{\rm obs}$ which is the rate expected from a random Poisson process over an observation time $T_{\rm obs}$. The resulting constraints are shown in Fig. 6 and will be discussed in Sec. IV.

C. Stochastic gravitational-wave background

Cosmic string networks also generate a stochastic background of GWs, which is measured using the energy density

$$\Omega_{\rm GW}(f) = \frac{f}{\rho_c}\frac{d\rho_{\rm GW}}{df}, \tag{25}$$

where $d\rho_{\rm GW}$ is the energy density of GWs in the frequency range f to $f + df$ and ρ_c is the critical energy density of the Universe. Following the method outlined in [56], the GW energy density is given by

$$\Omega_{\rm GW}^{(M)}(f; G\mu, p) = \frac{4\pi^2}{3H_0^2} f^3 \int_0^{h^*} dh h^2$$

$$\times \int_0^{+\infty} dz \frac{d^2 R^{(M)}}{dz dh}(h, z, f; G\mu, p), \tag{26}$$

where the spectrum is computed for a specific choice of free parameters $G\mu$ and p, and the maximum strain amplitude h^* is defined below. This equation gives the contribution to the stochastic background from the superposition of unresolved signals from cosmic string cusps and kinks, and we shall determine the total GW energy density due to cosmic strings is by summing the two. Note that this calculation *underestimates* the stochastic background since it only includes the high-frequency contribution from kinks and cusps. The low-frequency contribution from the smooth part of loops may be important, and has been discussed in [57–60]. Neglecting this contribution, conservative constraints will be derived.